Available online at www.sciencedirect.com
ScienceDirect
International Journal of Heat and Fluid Flow 28 (2007) 862–870
International Journal of HEAT AND FLUID FLOW
www.elsevier.com/locate/ijhff

A double-population lattice Boltzmann method with non-uniform mesh for the simulation of natural convection in a square cavity

F. Kuznik *, J. Vareilles, G. Rusaouen, G. Krauss

Thermal Sciences Center, National Institute of Applied Sciences Lyon, INSA – Bât FREYSSINET, 20 Av. A. Einstein – 69621 Villeurbanne Cedex, France

Received 7 February 2006; received in revised form 22 September 2006; accepted 20 October 2006
Available online 12 December 2006

Abstract

In this paper, a double-population thermal Lattice Boltzmann method has been proposed to solve the problem of the heated cavity with imposed temperatures. A Taylor series expansion – and least square – based Lattice Boltzamnn method (TLLBM) has been implemented in order to use a non-uniform mesh. This allowed to investigate, at reasonable computational cost, the laminar and transitional flow fields ($10^3 \leqslant Ra \leqslant 10^8$). The numerical results, concerning the heat and mass transfers in the cases tested, are in good agreement with those from the literature. This enables the use of such method for predicting thermal flows of engineering interest.

Keywords: Lattice Boltzmann method; Double-population; Non-uniform mesh; Natural convection; Square cavity; Laminar and transitional flows

1. Introduction

In the last two decades, the Lattice Boltzmann method (LBM) has proved its capability to simulate a large variety of fluid flows (Higuera et al., 1989; Benzi et al., 1992; Wolf-Gladrow, 2000; Succi, 2001; Filippova and Hanel, 2000; Mei et al., 2000; Lee and Lin (2001), ...). For the isothermal fluid flows, the LBM was found to be an accurate, stable and computationally "economic" method compared with classical computational fluid dynamics methods. The Lattice Boltzmann equation represents the minimal form of Boltzmann kinetic equation (Higuera and Jimenez, 1989), and the result is a very elegant and simple equation, for a discrete density distribution function $f_i(\vec{x},t) = f(\vec{x},\vec{c_i},t)$. This density distribution function represents the probability to find a particle at lattice site $\vec{x}$, at time t and moving with speed c_i.

The thermal LBM model has been investigated first by Massaioli et al. (1993). The main limitation of using LBM in engineering applications is the lack of satisfactory model for the thermal fluid flows problems. Three methods for solving thermal LBM exist: the multispeed approach, the passive scalar approach and the double-population approach. The multispeed approach consists in extending the distribution function in order to obtain the macroscopic temperature (Chen et al. (1994), Pavlo et al. (1998)). However, this approach requires much more computational effort because of the additional discrete speeds and suffers from numerical instabilities.

For the passive scalar approach, it consists in solving the velocity by the LBM and the macroscopic temperature equation independently. The macroscopic temperature equation is similar to a passive scalar evolution equation if the viscous heat dissipation and compression work done by pressure are negligible. The coupling to LBM is made by adding a potential to the distribution function equation. This approach enhances the numerical stability compared with multispeed approach (Crouse et al. (2002), D'Orazio et al. (2004)). The disadvantages are first the impossibility

* Corresponding author. Tel.: +33 472 438 459; fax: +33 472 438 522.
E-mail address: frederic.kuznik@insa-lyon.fr (F. Kuznik).

0142-727X/$ - see front matter © 2006 Elsevier Inc. All rights reserved.
doi:10.1016/j.ijheatfluidflow.2006.10.002

Nomenclature

$\vec{c}_i$	discrete particle speeds
c	lattice speed
dt	time increment
dx	lattice spacing
F	external forces
f, $\tilde{f}$	modified and original density distribution functions
g, $\tilde{g}$	modified and original internal energy distribution functions
f_i, g_i	discrete distribution functions
f_i^{e}, g_i^{e}	equilibrium discrete distribution functions
$\vec{G}$	buoyancy force per unit mass
$\vec{g}$	gravity
H	cavity size
Nu_0	average hot wall Nusselt number
Pr	Prandtl number
R	constant of the gas
Ra	Rayleigh number
t	time
T	temperature
$\vec{x} = (x, y)$	coordinates
$\vec{u} = (u, v)$	velocities

Greeks

β	coefficient of thermal expansion
ν	kinematic diffusivity
χ	thermal diffusivity
ρ	density
$\vec{\xi}$	absolute velocity
τ_v, τ_{c}	relaxation times

Superscripts and subscripts

c	cold
e	equilibrium
h	hot
m	mean
max	maximum

of incorporating the viscous heat dissipation and compression work done by pressure, and second the departure from the simplicity of LBM.

The double-population approach, used in this article, is based on the work of He et al. (1998). This model introduces an internal energy density distribution function in order to simulate the temperature field, the velocity field stilling simulated using the density distribution function. Compared with the multispeed thermal Lattice Boltzmann approach, the numerical scheme is numerically more stable. Moreover, this method is able to include the viscous heat dissipation and compression work done by pressure. Even if the method implies an overhead in terms of memory occupation compared with classical Navier–Stokes equations for the numerical simulation of complex flows, there is a gain concerning time-step size, which can be interesting as it has been noted in Rasin et al. (2005).

The validity of the model proposed in this article is done through its application to natural convection in the square cavity. The number of papers available shows the great interest in this topic. The flow is laminar for Rayleigh numbers (Ra) less than 10^6, the transition occurs for $10^6 < Ra < 10^8$ and the flow becomes fully turbulent for $Ra \geqslant 1.82 \cdot 10^8$. The numerical studies, used in this article, are, for the laminar flow, de Vahl Davis (1983) and Hortmann et al. (1990), and Markatos et al. (1984) and Le Quere (1991) for the transitional flow results.

Few researchers have carried out simulations of this flow using LBM. D'Orazio et al. (2004) simulated the natural convection in square cavity with Dirichlet and Neumann boundary conditions. Their study explored only the laminar flows. The main disadvantage of the method is the necessity of using regular lattice and then the requirement of enormous grid. In the present work, the Taylor series expansion – and least square – based Lattice Boltzmann method (TLLBM) of Shu et al. (2001) which allows to LBM with non-uniform grid, has been used. The TLLBM approach is completely meshless, compared with other non-uniform grid approaches. This method has been employed by Shu et al. (2002) for the square cavity problem. Again, the Rayleigh numbers simulated were limited to the laminar case only and with high grid size.

The present paper deals with the application of the thermal LBM developed by He et al. (1998) for the simulation of a Boussinesq fluid in a square cavity. To avoid the use of enormous grid, a non-uniform grid has been used, the implementation being held with the help of TLLBM. The main objective of this study is to validate the use of such model to predict the velocity and temperature fields in the case of natural convection in a square cavity for laminar and transitional flows.

2. The 2D incompressible thermal Lattice Boltzmann model

This part is devoted to an overview of the thermal Lattice Boltzmann model used (TLBM). The mathematical demonstration of the model can be found in He et al. (1998).

The main hypothesis of the TLBM are:

- Bhatnagar, Gross and Krook approximation (BGK) ⇒ the collision operator is expressed as a single relaxation time to the local equilibrium,
- the Knudsen number is assumed to be a small parameter,
- the flow is incompressible,

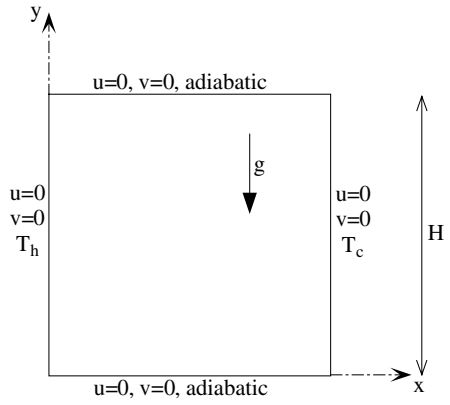

Fig. 1. Configuration of natural convection in a square cavity.

- the viscous heat dissipation and compression work done by pressure are neglected.

The evolution of the density distribution $\tilde{f}$ for a single fluid particle is then given by:

$$\frac{\mathrm{D}\tilde{f}}{\mathrm{D}t} = \partial_t \tilde{f} + (\vec{\xi}\cdot\nabla)\tilde{f} = -\frac{\tilde{f}-\tilde{f}^{\mathrm{e}}}{\tau_v} + F \tag{1}$$

$\vec{\xi}$ is the microscopic velocity, τ_v is the relaxation time, $\tilde{f}^{\mathrm{e}}$ the Maxwell–Boltzmann equilibrium distribution function and F the external forces.

Similarly, the internal energy distribution function $\tilde{g}$ is given by the following evolution equation:

$$\frac{D\tilde{g}}{Dt} = \partial_t \tilde{g} + (\vec{\xi}\cdot\nabla)\tilde{g} = -\frac{\tilde{g}-\tilde{g}^{\mathrm{e}}}{\tau_{\mathrm{c}}} \tag{2}$$

where τ_{c} is the relaxation time for the internal energy distribution function.

The macroscopic variables such as density ρ, velocity $\vec{u}$ and temperature T can be calculated as the moments of the distributions functions:

$$\rho(\vec{x},t) = \int \tilde{f}(\vec{x},\vec{\xi},t)\,\mathrm{d}\vec{\xi} \tag{3}$$

$$\rho(\vec{x},t)\vec{u}(\vec{x},t) = \int \vec{\xi}\tilde{f}(\vec{x},\vec{\xi},t)\,\mathrm{d}\vec{\xi} \tag{4}$$

$$\rho(\vec{x},t)RT = \int \tilde{g}(\vec{x},\vec{\xi},t)\,\mathrm{d}\vec{\xi} \tag{5}$$

with R the constant of the gas.

To obtain the Lattice Boltzmann model, the velocity space must be discretized: during $\mathrm{d}t$, the distribution function moves along the lattice link $\mathrm{d}\vec{x}_i = \vec{c}_i\,\mathrm{d}t$. In our simulations, a 9 velocities 2 dimensional (D2Q9) lattice has been used (see Fig. 2). Moreover, the density distributions f (Eq. (6)) and g (Eq. (7)) have been introduced by He et al. (1998) in order to avoid the implicitness of the second order scheme used to integrate the evolution equation.

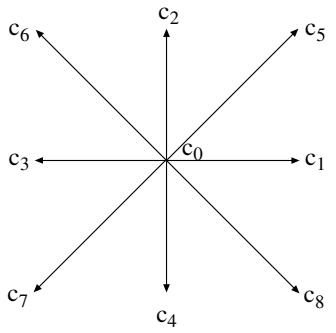

Fig. 2. The square lattice velocities $D2Q9$.

$$f = \tilde{f} + \frac{\mathrm{d}t}{2\tau_v}(\tilde{f}-\tilde{f}^{\mathrm{e}}) - \frac{\mathrm{d}t}{2}F \tag{6}$$

$$g = \tilde{g} + \frac{\mathrm{d}t}{2\tau_{\mathrm{c}}}(\tilde{g}-\tilde{g}^{\mathrm{e}}) \tag{7}$$

After discretization, the evolution equations become:

$$f_i(\vec{x}+\vec{c}_i\mathrm{d}t, t+\mathrm{d}t) + f_i(\vec{x},t) = -\frac{\mathrm{d}t}{\tau_v+0.5\,\mathrm{d}t}(f_i - f_i^{\mathrm{e}}) + \frac{\mathrm{d}t\tau_v}{\tau_v+0.5\,\mathrm{d}t}F_i \tag{8}$$

$$g_i(\vec{x}+\vec{c}_i\,\mathrm{d}t, t+\mathrm{d}t) + g_i(\vec{x},t) = -\frac{\mathrm{d}t}{\tau_{\mathrm{c}}+0.5\,\mathrm{d}t}(g_i - g_i^{\mathrm{e}}) \tag{9}$$

For the two dimensional case, applying the third-order Gauss-Hermite quadrature leads to the D2Q9 model with the following discrete velocities $\vec{c}_i$ with $i = 1,\ldots,8$ and $\vec{c}_0 = 0$:

$$\vec{c}_i = \left(\cos\left(\frac{\mathrm{i}-1}{4}\pi\right), \sin\left(\frac{\mathrm{i}-1}{4}\pi\right)\right)c \tag{10}$$

where $c = \sqrt{3RT_m}$ (to improve numerical stability, T_{m} is the mean value of temperature for the calculation of c). The equilibrium density distribution function is given by:

$$f_i^{\mathrm{e}} = \omega_i\rho\left[1 + 3\frac{\vec{c}_i\cdot\vec{u}}{c^2} + 4.5\frac{(\vec{c}_i.\vec{u})^2}{c^4} - 1.5\frac{(u^2+v^2)}{c^2}\right] \tag{11}$$

with $\vec{u} = (u,v)$ and $\omega_0 = 4/9$, $\omega_i = 1/9$ for $i = 1, 2, 3, 4$, $\omega_i = 1/36$ for $i = 5, 6, 7, 8$.

The equilibrium internal energy density function can be written as:

$$g_0^{\mathrm{e}} = -\frac{2}{3}\rho e\frac{(u^2+v^2)}{c^2} \tag{12}$$

$$g_i^{\mathrm{e}} = \omega_1\rho e\left[1.5 + 1.5\frac{\vec{c}_i.\vec{u}}{c^2} + 4.5\frac{(\vec{c}_i.\vec{u})^2}{c^4} - 1.5\frac{(u^2+v^2)}{c^2}\right] \tag{13}$$

for $i = 1, 2, 3, 4$.

$$g_i^{\mathrm{e}} = \omega_2\rho e\left[3 + 6\frac{\vec{c}_i.\vec{u}}{c^2} + 4.5\frac{(\vec{c}_i.\vec{u})^2}{c^4} - 1.5\frac{(u^2+v^2)}{c^2}\right] \tag{14}$$

for $i = 5, 6, 7, 8$.

Finally, the macroscopic variables ρ, $\vec{u}$ and T can be calculated using:

$$\rho = \sum_i f_i \tag{15}$$

$$\rho\vec{u} = \sum_i \vec{c}_i f_i - \frac{\mathrm{d}t}{2}\vec{G} \tag{16}$$

$$\rho RT = \sum_i g_i \tag{17}$$

where $\vec{G}$ is the external force acting per unit mass.

Using a Chapman–Enskog expansion, the Navier–Stokes equations can be recovered with the described model. The kinematic viscosity v and the thermal diffusivity χ are then related to the relaxation times by:

$$v = \frac{\tau_v c^2}{3} \tag{18}$$

$$\chi = \frac{2\tau_c c^2}{3} \tag{19}$$

3. Buoyancy force and dimensionless parameters

To demonstrate the validity of the thermal Lattice Boltzmann approach proposed, simulations on the square cavity are hold. This test-case is described Fig. 1. With the Boussinesq approximation, all the fluid properties are considered as constant, except the body force term in the Navier–Stokes momentum equation where the fluid density is given by $\rho = \rho_m(1 - \beta(T - T_m))$, where ρ_m is the average fluid density, T_m the average fluid temperature and β the thermal coefficient expansion of the fluid. In that case, the external force acting per unit mass $\vec{G} = -\rho\beta(T - T_m)\vec{g}$, and the external force F_i appearing in Eq. (8) is given by:

$$F_i = \frac{3\vec{G}.(\vec{c}_i - \vec{u})}{c^2} f_i^e \tag{20}$$

The major control parameter of the test-case is the Rayleigh number $Ra = \beta g(T_h - T_c)H^3 Pr/v^2$ with $Pr = v/\chi$. To ensure that the code works in near incompressible regime, the characteristic velocity of the flow $\sqrt{\beta g(T_h - T_c)H}$ must be small compared with the fluid speed of sound. In our simulations, we chose a factor of 10 between these velocities.

All the velocities are normalized using the diffusion velocity $v^* = vPr/H$. The temperatures are dimensionless parameters using $\frac{T-T_c}{T_h-T_c}$. The x and y dimensions are normalized using H.

4. Implementation on non-uniform grid

In traditional LBM, the grid is defined as a regular lattice with equal spaces. But for high Rayleigh number flows, the thermal boundary layer is very thin and then requires considerable number of nodes, wasting computational time and memory size. The Taylor series expansion – and least square – based lattice Boltzmann method (TLLBM) of Shu et al. (2001) is based on the fact that distribution functions are continuous functions in the physical space and can be defined in any mesh system: it allows mesh refinement near the walls. Even if this method is in theory meshless, we use a based non-uniform grid in order to have a more simple algorithm script.

Let us consider a point which position is $\vec{x}_0$ and M neighboring points which positions are $\vec{x}_k$, $k = 1 \ldots M$. If the distribution functions are known for all points at time t, the TLLBM allows to calculate the distribution functions at $\vec{x}_0$ for time $t + \mathrm{d}t$ with the help of the neighboring points. When TLLBM is applied to the evolution Eq. (8) and (9), the final form is:

$$f_i(\vec{x}_0, t + \mathrm{d}t) = \sum_{k=1}^{k=M+1} a_{1,k} f'_{k-1} \tag{21}$$

$$g_i(\vec{x}_0, t + \mathrm{d}t) = \sum_{k=1}^{k=M+1} a_{1,k} g'_{k-1} \tag{22}$$

where

$$f'_k = f_i(\vec{x}_k, t) - \frac{\mathrm{d}t}{\tau_v + 0.5\,\mathrm{d}t}\left(f_i(\vec{x}_k, t) - f_i^e(\vec{x}_k, t)\right) + \frac{\tau_v\,\mathrm{d}t}{\tau_v + 0.5\,\mathrm{d}t} F_i(\vec{x}_k, t) \tag{23}$$

$$g'_k = g_i(\vec{x}_k, t) - \frac{\mathrm{d}t}{\tau_c + 0.5\,\mathrm{d}t}\left(g_i(\vec{x}_k, t) - g_i^e(\vec{x}_k, t)\right) \tag{24}$$

$a_{1,k}$ is the first row of the matrix A, which is calculable with the geometry of mesh point: A must be calculated only once during the simulation. The formation of the geometric matrixes can be found in Shu et al. (2005). In order to avoid ill-conditioning matrixes, $M > 5$. As we used a base structured grid, $M = 8$ considering the 8 neighboring of each point.

5. Boundary conditions

For the square cavity, the no-slip boundary condition is imposed at the walls. The vertical walls have constant temperatures. The condition on the adiabatic horizontal walls is converting into a Dirichlet boundary condition using a second order finite-difference approximation.

Implementation of boundary conditions is very important for the simulation. The unknown distribution functions pointing to the fluid zone at the boundaries nodes must be specified. Concerning the no-slip boundary condition, the bounce-back rule of the non-equilibrium distribution function developed by Zhou and He (1997) is used.

The unknown density distribution functions at the boundary can be determined by the following condition:

$$f_\alpha - f_\alpha^e = f_\beta - f_\beta^e \tag{25}$$

where $\vec{e}_\alpha$ and $\vec{e}_\beta$ have opposite directions, $\vec{e}_\alpha$ being the direction where the distribution function is unknown and $\vec{e}_\beta$ the direction of the known distribution function. To reinforce the no-slip boundary condition, the velocity at the wall is used in the calculation of the density equilibrium functions.

Table 1
Grid dependence study for the case $Ra = 10^4$

Mesh	32×32	64×64	96×96	128×128	160×160	de Vahl Davis (1983)
u_{max}	15.294	15.958	16.142	16.167	16.192	16.178
y_{max}	0.807	0.826	0.824	0.821	0.821	0.823
v_{max}	18.304	19.335	19.559	19.597	19.623	19.617
x_{max}	0.130	0.123	0.120	0.120	0.120	0.119
Nu_0	2.187	2.281	2.245	2.246	2.246	2.238

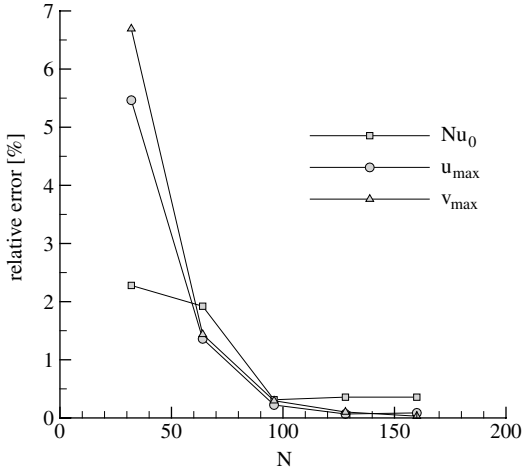

Fig. 3. Numerical error for Nu_0, u_{max} and v_{max} versus grid size for $Ra = 10^4$.

Similarly, the internal energy distribution functions can be determined with the following condition:

$$g_\alpha - g_\alpha^e - \vec{e}_\alpha^2(f_\alpha - f_\alpha^e) = g_\beta - g_\beta^e - \vec{e}_\beta^2(f_\beta - f_\beta^e) \quad (26)$$

The wall temperatures are used for the calculation of the internal energy equilibrium functions.

At the corner of the boundary, there exist some special particle which do not go from the outside environment into the flow field. For example, for the top-left corner, such special directions are $\vec{c}_5$ and $\vec{c}_7$. As the values of distributions functions are necessary for these directions when applying TLLBM, they are calculated by using a second order extrapolation scheme with interior points.

6. Numerical simulation

The program has been written in C, using numerical methods coming from Press et al. (1992). The overview of the algorithm can be decomposed as follow:

(1) create the grid geometry and calculate the TLLBM matrixes coefficients,
(2) initialize distribution functions,
(3) impose boundary conditions,

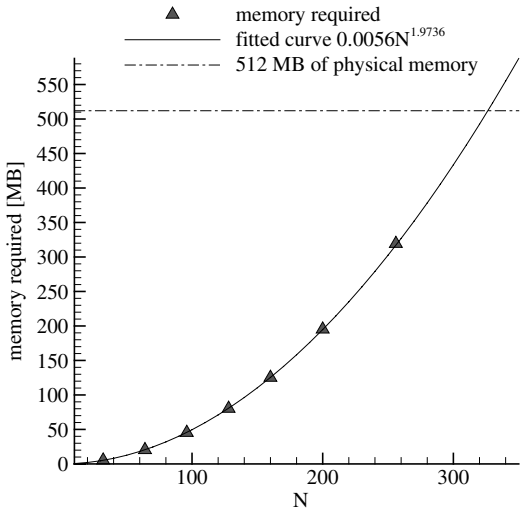

Fig. 4. Memory consumption as a function of the size of the computational domain for the code proposed (symbols) and the fitted curve (solid). The dot-dashed line represents the amount of memory available on a typical small workstation.

Table 2
Comparison of laminar flow with previous works for the square heated cavity with imposed temperatures

		$Ra = 10^3$	$Ra = 10^4$	$Ra = 10^5$	$Ra = 10^6$
u_{max}	de Vahl Davis (1983)	3.649	16.178	34.730	64.630
	Hortmann et al. (1990)	–	16.180	34.740	64.837
	Present	3.636	16.167	34.962	64.133
y_{max}	de Vahl Davis (1983)	0.813	0.823	0.855	0.850
	Hortmann et al. (1990)	–	0.825	0.837	0.850
	Present	0.809	0.821	0.854	0.860
v_{max}	de Vahl Davis (1983)	3.697	19.617	68.590	219.360
	Hortmann et al. (1990)	–	19.629	68.639	220.461
	Present	3.686	19.597	68.578	220.537
x_{max}	de Vahl Davis (1983)	0.178	0.119	0.066	0.038
	Hortmann et al. (1990)	–	0.120	0.883	0.039
	Present	0.174	0.120	0.067	0.038
Nu_0	de Vahl Davis (1983)	1.117	2.238	4.509	8.817
	Hortmann et al. (1990)	–	2.244	4.521	8.825
	Present	1.117	2.246	4.518	8.792

(4) collision operation which consists in the calculation of f',
(5) propagation operation which consists in the calculation of distribution function at $t + \mathrm{d}t$,
(6) test the convergence criterion, if false return to step (3).

The simulations are held for Rayleigh numbers from 10^3 to 10^8. The non-uniform grid is used for $Ra > 10^4$. The convergence criterion for all the cases tested is:

$$\max_{\text{grid}} \left| \sqrt{(u^2+v^2)^{n+1}} - \sqrt{(u^2+v^2)^{n}} \right| \leqslant 10^{-7} \tag{27}$$

$$\max_{\text{grid}} \left| T^{n+1} - T^{n} \right| \leqslant 10^{-7} \tag{28}$$

7. Results and discussion

The comparisons with the literature results are held for $10^3 \leqslant Ra \leqslant 10^8$ and $Pr = 0.71$. Among the characteristic numerical values of the flow, the comparisons concern the average Nusselt number at the hot wall, the maximum horizontal velocity and the maximum vertical velocity, with the positions where they occur.

The average Nusselt number at the hot wall, Nu_0, is calculated via:

$$Nu_0 = -\frac{1}{(T_h - T_c)} \int_0^H \left. \frac{\partial T}{\partial x} \right|_{\text{hot wall}} \mathrm{d}y \tag{29}$$

where the temperature gradient is obtained using a second-order scheme.

The maximum horizontal velocity $u_{\max}$ is obtained for $y = 0.5$ at $x_{\max}$; the maximum vertical velocity $v_{\max}$ is given at $x = 0.5$ and $y_{\max}$.

7.1. Grid dependence

The grid dependence study of the results is examined before the comparisons. The case $Ra = 10^4$ has been chosen with a regular lattice which dimensions are $N \times N$, with N the number of grid points. Five grid size have been tested and the results are summarized in Table 1. These results show that when N increases, the calculated values quickly approach the values given by the benchmark of de Vahl Davis (1983). Fig. 3 presents the relative errors, in percent, of the calculated values of Nu_0, $u_{\max}$ and $v_{\max}$ versus the grid size N. From this figure, there is no much improvement in the results when N increases from 128 to 160.

For grid dependence studies, the following grid size have been chose:

- for $Ra = 10^3$, 64×64 with uniform grid,

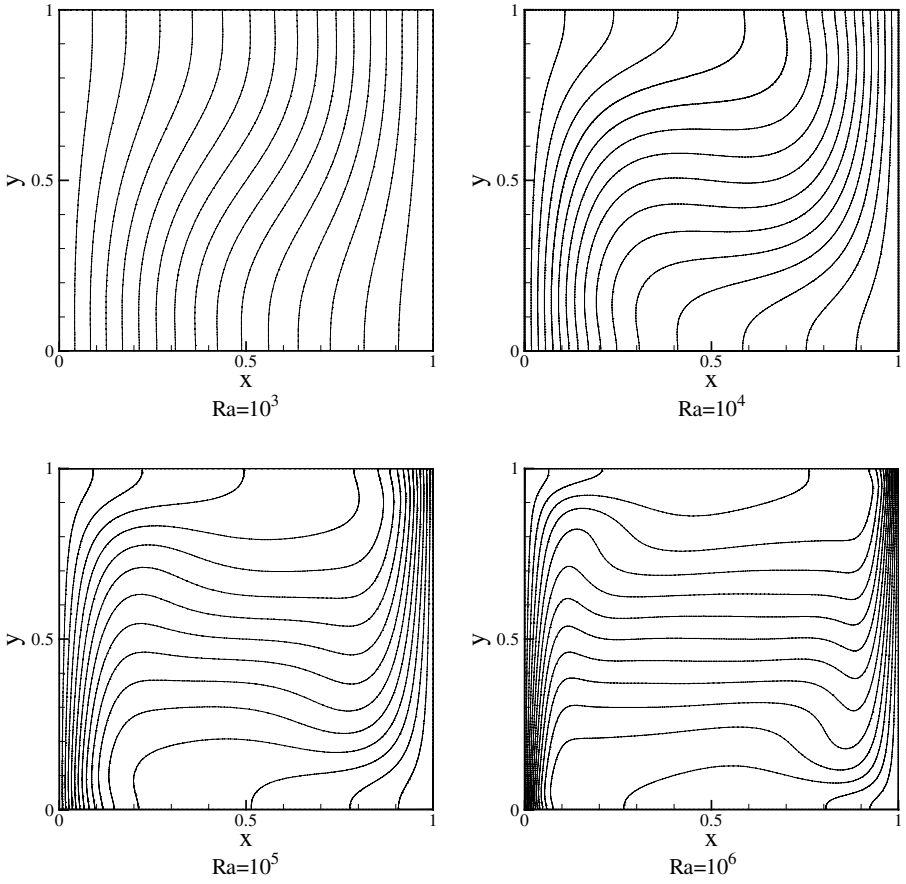

Fig. 5. Isotherms for the laminar flow.

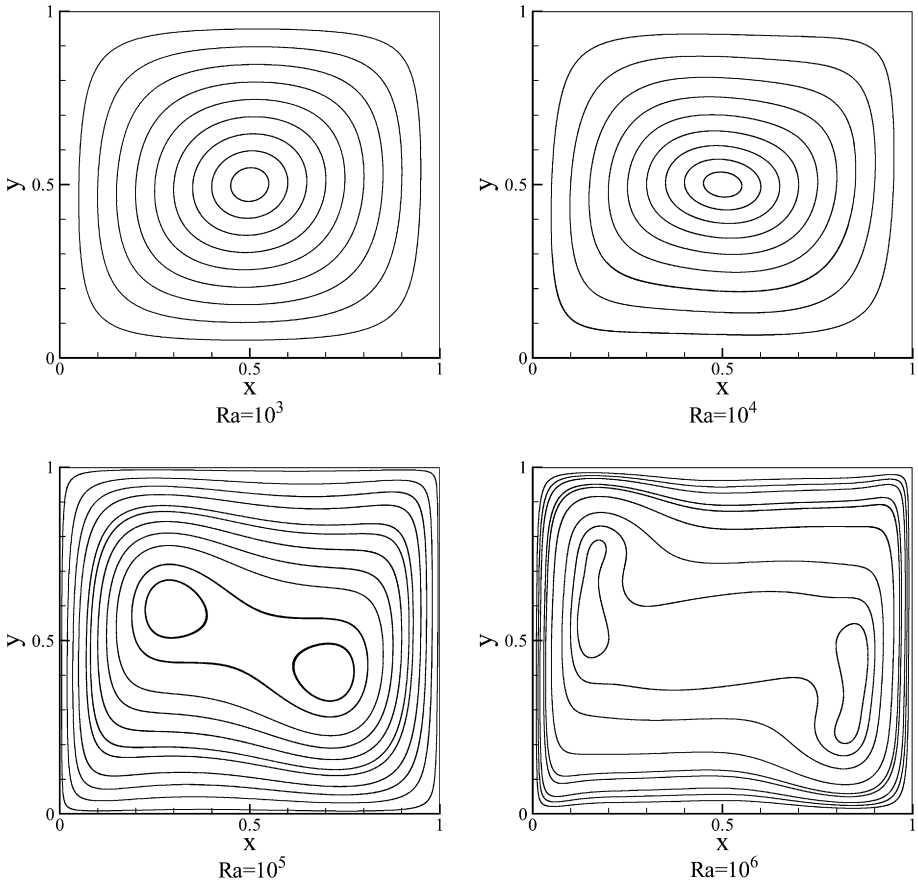

Fig. 6. Streamlines for the laminar flow.

- for $Ra = 10^4$, 128×128 with uniform grid,
- for $Ra = 10^5$, 128×128 with non-uniform grid (which requires 200×200 with uniform grid),
- for $Ra = 10^6$, 128×128 with non-uniform grid (which requires 250×250 with uniform grid),
- for $Ra = 10^7$, 256×256 with non-uniform grid (which requires 510×510 with uniform grid),
- for $Ra = 10^8$, 256×256 with non-uniform grid (which requires 1150×1150 with uniform grid).

7.2. Memory requirement and calculation time

All the simulations have been made using a personal computer with a P4 1.7 GHz processor. Numerical simulation programs using Lattice Boltzmann methods are limited in the range of problems they can address by memory requirements. For solving $Ra = 10^6$, 128×128 with non-uniform grid, 80.29 MB of memory are needed. The Fig. 4 shows the memory consumption for the code proposed and the fitted curve. From this figure, the total memory required is approximatively a function of N^2.

The TLLBM method needs more calculation time than standard LBM method with uniform grid concerning the same grid. However, for a given Ra, the TLLBM method takes less grid points than the LBM method and then less calculation time. For $Ra = 10^3$, the calculation time needed to get the convergence is 186 s. For $Ra = 10^5$, it takes 18,128 s to get the convergence with non-uniform grid 128×128. With LBM method with uniform mesh, the grid size must be 200×200 to get the same accuracy as TLLBM and the calculation time becomes 30,817 s.

Table 3
Comparison of transitional flow with previous works for the square heated cavity with imposed temperatures

		$Ra = 10^7$	$Ra = 10^8$
u_{max}	Markatos et al. (1984)	–	514.3
	Le Quere (1991)	148.580	321.876
	Present	148.768	321.457
y_{max}	Markatos et al. (1984)	–	0.941
	Le Quere (1991)	0.879	0.928
	Present	0.881	0.940
v_{max}	Markatos et al. (1984)	–	1812
	Le Quere (1991)	699.236	2222.39
	Present	702.029	2243.36
x_{max}	Markatos et al. (1984)	–	0.0135
	Le Quere (1991)	0.021	0.120
	Present	0.020	0.121
Nu_0	Markatos et al. (1984)	–	32.045
	Le Quere (1991)	16.523	30.225
	Present	16.408	29.819

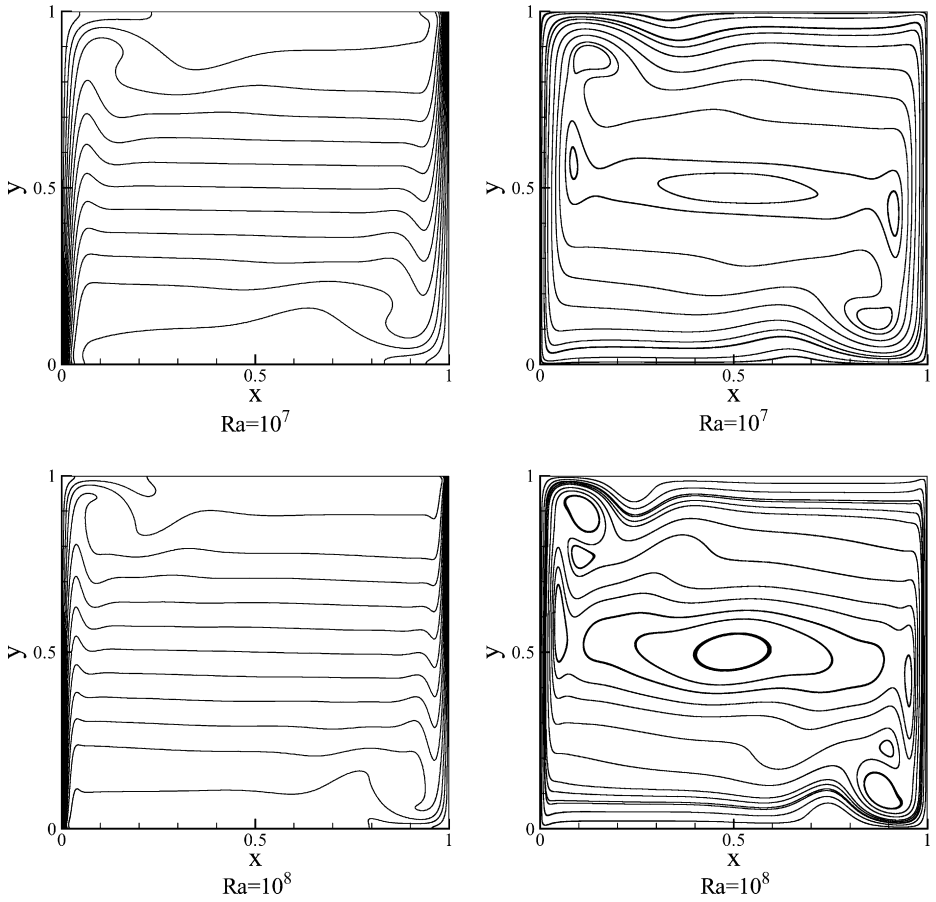

Fig. 7. Isotherms (left) and streamlines (right) for the transitional flow.

7.3. Numerical results

The details concerning the flow fields for the square heated cavity can be found in the literature. The transition from the motionless conduction dominated regime to the convection dominated regime takes place after $Ra = 10^3$. For $10^7 \leqslant Ra \leqslant 10^8$, the fluid motion takes place at the boundary layer near the walls. The results analysis will be divided in two parts: the laminar flow and the transitional flow.

7.4. The laminar flow $10^3 \leqslant Ra \leqslant 10^6$

Table 2 reports the average Nusselt number at the hot wall, the maximum vertical velocity, the maximum horizontal velocity and the positions where they occur. The numerical results obtained with the Lattice Boltzmann method described in this paper are very close to the values found in the literature (the maximum relative error is about 1%).

Figs. 5 and 6 show respectively the isotherms and streamlines for the laminar flow cases. As the Rayleigh number increases, the fluid motion mainly takes place near the differentially heated walls and the flow in the core of the cavity becomes quasi-motionless: these flow features are well captured by the numerical method proposed.

7.5. The transitional flow $10^7 \leqslant Ra \leqslant 10^8$

One of the main interest of this paper is to prove that the transitional flow can be simulated using Lattice Boltzmann method with non-uniform mesh at a low computational cost. Table 3 summarizes the numerical values of Nu_0, u_{max}, v_{max}, x_{max} and y_{max} compared with literature results. From this table, the numerical values are in good agreement with those from literature: the relative error, compared with the results of Le Quere (1991), is less than 1.5% for all the values reported.

The isotherms and streamlines for the transitional flow are shown in Fig. 7. The temperature field is becoming more and more stratified, with horizontal streamlines. Moreover, reversed flows occur at upper-left and bottom-right corners, destabilizing the laminar flow: the transitional flow features are well captured by our model.

8. Conclusions

A thermal Lattice Boltzmann model with non-uniform grid implementation has been discussed. Compared with

previous studies, the TLLBM allows to reduce the mesh grid necessary to solve the Boltzmann problem. Moreover, the double population approach has shown its capability to solve the heat transfer problem in the case of the heated square cavity, until $Ra = 10^8$.

The main advantage of lattice Boltzmann method, which has not been tested in this article, is that the high parallelism of such algorithm. This allow to use such method for the computation of higher complexity fluid flows: it makes lattice Boltzmann methods competitive tools, compared with standard numerical techniques.

The main problem for the simulations of fluid flows is the modelling of turbulence (more explanations about the methods can be found in Chen et al. (2003)). The next step of our work is to introduce, in the lattice Boltzmann method described in this paper, a Large Eddy Simulation modelling of turbulence. The turbulent dissipative effects are then interpreted as an eddy viscosity associated to a turbulent relaxation time calculated with the help of a lattice Boltzmann stress tensor.

References

Benzi, R., Succi, S., Vergassola, M., 1992. The lattice Boltzmann equation: theory and applications. Phys. Rep. 222, 145–197.

Chen, Y., Ohashi, H., Akiyama, M.A., 1994. Thermal lattice Bhatnagar–Gross–Krook model without nonlinear deviations in macrodynamic equations. Phys. Rev. E 50, 2776–2783.

Chen, H., Kandasamy, S., Orszag, S., Shock, R., Succi, S., Yakhot, V., 2003. Extended Boltzmann Kinetic Equation for Turbulent Flows. Science 301, 633–636.

Crouse, B., Krafczyk, M., Kuhner, S., Rank, E., Van Treeck, C., 2002. Indoor air flow analysis based on lattice Boltzmann methods. Energy Build 34, 941–949.

de Vahl Davis, G., 1983. Natural convection of air in a square cavity: a bench mark numerical solution. Int. J. Numer. Meth. Fluids 3, 249–264.

D'Orazio, A., Corcione, M., Cielata, G.P., 2004. Application to natural convection enclosed flows of a lattice Boltzmann BGK model coupled with a general purpose thermal boundary condition. Int. J. Thermal Sci. 43, 575–586.

Filippova, O., Hanel, D., 2000. A novel BGK approach for low Mach number combustion. J. Comput. Phys. 158, 139–160.

He, X., Chen, S., Doolen, G.D., 1998. A novel thermal model for the lattice Boltzmann method in incompressible limit. J. Comput. Phys. 146, 282–300.

Higuera, F.J., Jimenez, J., 1989. Boltzmann approach to lattice gas simulation. Europhy. Lett. 9, 663–668.

Higuera, F.J., Succi, S., Benzi, R., 1989. Lattice gas dynamics with enhanced collisions. Europhys. Lett 9, 345–349.

Hortmann, M., Peric, M., Scheuerer, G., 1990. Finite volume multigrid prediction of laminar natural convection: bench-mark solutions. Int. J. Numer. Meth. Fluids 11, 189–207.

Lee, T., Lin, C.L., 2001. A characteristic Galerkin method for discrete Boltzmann equation. J. Comput. Phys. 171, 336–356.

Le Quere, P., 1991. Accurate solutions to the square thermally driven cavity at high Rayleigh number. Comput. Fluids 20, 29–41.

Markatos, N.C., Pericleous, 1984. Laminar and turbulent natural convection in an enclosed cavity. Int. J. Heat Mass Transfer 27, 755–772.

Massaioli, F., Benzi, R., Succi, S., 1993. Exponential tails in two-dimensionnal Rayleigh–Bénard convection. Europhys. Lett. 21, 305–310.

Mei, R., Shyy, W., Yu, D., Luo, L.S., 2000. Lattice Boltzmann method for 3-D flows with curved boundary. J. Comput. Phys. 161, 680–699.

Pavlo, P., Vahala, G., Vahala, L., Soe, M., 1998. Linear-stability analysis of thermo-lattice Boltzmann models. J. Comput. Phys. 139, 79–91.

Press, W.H., Teukolsky, S.A., Vatterling, W.T., Flannery, B.P., 1992. Numerical Recipes in C – The Art of Scientific Computing, second ed. Cambridge University Press, 994p.

Rasin, I., Succi, S., Miller, W., 2005. A multi-relaxation lattice method for passive scalar diffusion. J. Comput. Phys. 206, 452–453.

Shu, C., Chew, Y.T., Niu, X.D., 2001. Least square-based LBM: a meshless approach for simulation of flows with complex geometry. Phys. Rev. E 64, 1–4.

Shu, C., Peng, Y., Chew, Y.T., 2002. Simulation of natural convection in a square cavity by Taylor series expansion- and least squares-based Lattice Boltzmann method. Int. J. Mod. Phys. C 13, 1399–1414.

Shu, C., Niu, X.D., Chew, Y.T., Peng, Y., 2005. Taylor series expansion – and least square – based lattice Boltzmann method: an efficient approach for simulation of incompressible viscous flows. Prog. Comput. Fluid Dyn. 5, 27–36.

Succi, S., 2001. The Lattice Boltzmann – For Fluid Dynamics and Beyond. Oxford University Press, 288p.

Wolf-Gladrow, D.A., 2000. Lattice-Gas Cellular Automata and Lattice Boltzmann Models: An Introduction. Springer, Berlin, 308p.

Zhou, Q., He, X., 1997. On pressure and velocity boundary conditions for the lattice Boltzmann BGK model. Phys. Fluids 9, 1591–1598.